

# A Field Guide to BRDF Models\*

Stephen H. Westin Hongsong Li Kenneth E. Torrance

PCG-04-1

January, 2004

We present a principled approach to selecting a surface reflectance model and setting its parameters. The approach is based on fundamental physical principles, comparisons between different models, and practical insight into the characteristics of real surfaces. Four models of surface reflectance were evaluated by comparing them with physical measurements on five different sample surfaces. Conclusions are drawn about which of the models are best to represent different surfaces, since no one model was a clear winner in all cases. Principles and visual checks are derived to help practitioners model a variety of surfaces with good accuracy.

\*This report was submitted for publication at SIGGRAPH 2004.

# A Field Guide to BRDF Models

Category:

## Abstract

We present a principled approach to selecting a surface reflectance model and setting its parameters. The approach is based on fundamental physical principles, comparisons between different models, and practical insight into the characteristics of real surfaces. Four models of surface reflectance were evaluated by comparing them with physical measurements on five different sample surfaces. Conclusions are drawn about which of the models are best to represent different surfaces, since no one model was a clear winner in all cases. Principles and visual checks are derived to help practitioners model a variety of surfaces with good accuracy.

## 1 Introduction

In reproducing the appearance of real-world surfaces in computer renderings, practitioners have been forced to depend on a combination of experience, intuition, and cut-and-try experimentation. To avoid this process, [Borshukov 2003] used detailed reflectance measurements, but this is only practical if the user has access to specialized measurement equipment. This paper seeks to provide a third way by providing a few guidelines, based on detailed physical measurement and comparisons, which can be applied based on visual observations of a surface.

Historically, there has been a gulf between theory and practice in modeling surface reflectance for computer rendering. Models of surface reflectance range from empirical models that “look right” under the proper conditions to elaborate models of the optical processes involved. Researchers have continued to develop and refine models, while practitioners still face the problem of selecting a model and tuning its parameters empirically.

This paper is a start toward bridging that gap between theory and practice. Rather than proposing a new model or representation, this paper provides new insights into how to use models that already exist.

There are two new insights in this paper: the relative performance of several well-known models on a number of different surfaces, and guidelines on setting model parameters based on visual observations of a surface. To do the first, we chose several well known models and a number of test cases that show where each model is most applicable. We use physical measurements to provide a standard by which to judge the ability of each model to reproduce real-world surfaces, making test renderings to show the visual significance of the differences between models and then interpreting the results based on a basic understanding of the physics of surface reflection. For the second, we use an understanding of the physical processes involved to provide guidelines for converting simple visual observations to approximate model parameters.

Our approach is to measure the BRDF of several carefully-chosen samples in the plane of incidence, fitting four different well-known models to each set of data. We then explain the phenomena found in each dataset in light of the physical processes involved, assess each model on its fidelity to the original data, and relate these phenomena and modeling differences to their visual effect in a rendered image. This approach combines the generality of a theoretical, technical approach with the concrete applicability of the empirical approach.

We feel this is a more robust method than either the measurements or the renderings alone, as we take a wide range of incidence and reflection angles into account. A test image, no matter how carefully designed, cannot show all possible incidence/reflection combinations, and so could potentially miss effects that will be visible in some other image.

We will start by reviewing the history of reflectance modeling for computer rendering, elucidate some relevant principles of surface optics, then present five sample surfaces, comparing how four different models capture the reflectance behavior of each. Finally we will draw some simple guidelines, based on these principles and examples, to aid in the selection of a suitable reflectance model for a given surface.

## **2 Background**

Researchers have taken three main approaches to modeling reflectance for computer renderings: simple empirical models, physically-based models, and general mathematical fitting representations.

The earliest realistic computer renderings used a simple Lambertian model, limiting environments to purely diffuse surfaces. Phong [1975] introduced an empirical model that dramatically improved the richness and realism of rendered images. His model was designed to reproduce a glossy effect with minimal computation, and provided three simple parameters to control the appearance visually. Since then, Ward created a model almost as simple and efficient [Ward 1992], but designed to fit measured reflectance data and to incorporate effects of surface anisotropy. The Phong model itself has been modified to obey certain physical laws to allow use in simulations of global illumination [Lewis 1993]. More recently, Westlund and Meyer [2001] developed an empirical model based on traditional gloss and appearance measurements.

These models are compact and computationally efficient, and most offer a small number of parameters that can be manipulated interactively to achieve a desired appearance. They may fall short in reproducing the exact reflectance of a surface, but there is controversy as to how visually important such errors may be.

Physically-based models were introduced to computer rendering by Blinn [1977] and Cook and Torrance [1982]. This was followed by several partial models of physical scattering processes including the anisotropic models of Kajiya [Kajiya 1985] and Poulin and Fournier [1990]. Oren and Nayar [1994] presented a model for extremely rough surfaces such as unglazed ceramics. Finally, there are models of complete wave optics for certain classes of surfaces [He et al. 1991; Stam 1999].

These models offer the hope of very accurate modeling of surface reflectance, but how is one to set the physical parameters needed by these models? These parameters often have no direct intuitive meaning and require special equipment to measure. This means that the models are unsuited to interactive use.

The final class of reflectance models is that of general mathematical fitting representations. Since the reflectance is a function of 3 or 4 geometric variables, it is possible to construct a representation for fitting based on orthographic basis functions. Sillion et al. [1991] and Westin et al. [1992] used spherical harmonics as a basis set on the unit sphere; Koenderink and van Doorn [1998] used the Zernike polynomials in a similar fashion. Schröder and Sweldens [1995] and Lalonde and Fournier [1997] used wavelets. Kautz and McCool [1999] have represented the BRDF as a sum of separable functions. These representations share two features: each is theoretically capable of representing any BRDF exactly, and they require many

coefficients (dozens, hundreds, or even thousands) to achieve a good approximation of a typical BRDF, as compared to 3-4 coefficients for models in the other two categories. Lafortune et al.[1997] struck a middle ground by generalizing the Phong model with multiple steerable lobes. This model sacrifices the complete generality of other models in this category, but is much simpler and more compact ( $\leq 10$  coefficients). A different approach was used by Matusik et al.[2003], attempting to enumerate the entire space of BRDFs occurring in the real world and extracting a relatively small number (15-30) of basis functions to span the space.

Practically speaking, these general representations must be fit to data from another source: either a physical model or measured data. It is telling that each of these papers either includes its own set of measurements or relies on some of the few BRDF datasets publicly available[Dana et al. 1997; Cornell University Program of Computer Graphics 1999]. Not only are the parameters too numerous, but they lack any intuitive meaning. The empirical models such as Phong are designed to be controlled interactively, and even the physically-based models can be worked with, as they are controlled by a few physically-based parameters.

All this work, it seems, has benefited us little; current commercial rendering systems seem to offer little that was invented after 1980. Publication of a new model is generally accompanied by impressive renderings, but little comparison with the growing number of alternative models. Many models are evaluated for their physical accuracy, without establishing whether this results in visible improvement in the final image. Practitioners are forced to make a choice based on intuition, experience, and the limitations of a particular renderer.

### **3 Making Surface Optics Comprehensible**

Reflection of light from surfaces is a very complex subject, but we can gain much understanding by restricting our domain and introducing a few simple principles. We can use these principles to characterize many surfaces, as we will demonstrate in Section 4.

### **3.1 Domain of Application**

This paper deals only with a certain class of surfaces, those that

- can be treated as opaque
- can be described well by pure height fields
- are rough in a random way
- are isotropic in roughness
- range from perfectly smooth to quite rough
- display only certain types of subsurface scattering

By “opaque”, we mean that a surface displays no visible translucence. This means that any light scattered beneath the surface must be absorbed or reemitted within a region of the surface small with respect to the scale of depiction.

A surface that can be described as a pure height field has a well-defined interface, unlike, say, hair or velvet.

Random roughness means that the features on the surface are distributed with no regular structure. A diffraction grating is rough, but not random. A sandblasted surface has random roughness.

An isotropic surface displays reflectance invariant with respect to rotation about the surface normal. Most paints and papers, most plastics, and metal that has been sandblasted or shot-blasted are usually isotropic. Anisotropic surfaces include wood and brushed metal.

The range of surface roughness we deal with is quite wide, ranging from mirrors to uncoated paper and other rougher surfaces.

We restrict the types of subsurface scattering because good models for subsurface scattering are rare. Most of our examples show subsurface scattering that can be treated as Lambertian, but we include a more interesting metallic paint sample.

These limitations may seem to be quite restrictive, but they actually embrace a broad array of surfaces encountered in normal life. The examples in this paper include plastic and painted surfaces, metal surfaces,

and even high-gloss metallic automotive paint.

## 3.2 A Few Basic Principles

Real-world surfaces, even within our chosen domain, display a wide variety of reflectance phenomena, but most can be described in terms of a few processes and phenomena. This section explains the most important for our domain.

### 3.2.1 Metals vs. Dielectrics

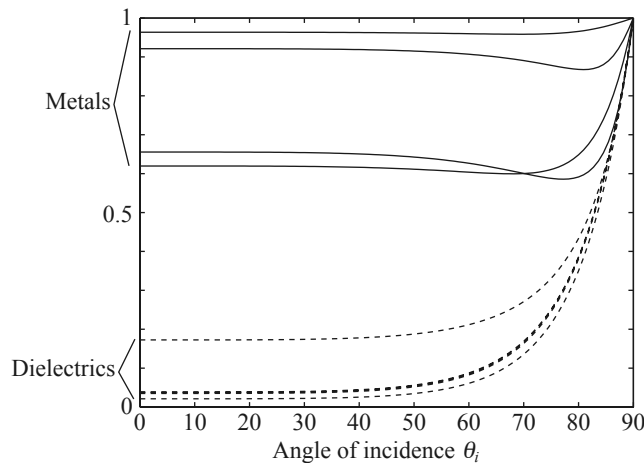


Figure 1: Fresnel reflectance for smooth surfaces: metals vs. dielectrics

Almost all materials can be separated into two categories: metals and dielectrics. Metals conduct electricity; dielectrics do not. There is also a class of semiconductors which we will ignore, as they are rare in practice. We are accustomed to making the distinction every day; we can almost always tell whether a surface is made of metal or not by looking at it, because metallic surfaces have a distinct appearance that is due entirely to their electrical conductivity. Reflectance from a smooth metal surface is relatively independent of angle, while dielectrics have low reflectance over most of the angular range with a steep increase near grazing, as shown in Figure 1. The metals all show a reflectance of over 50% for all angles, while the dielectrics fall below 20% for the majority of the range. Though Figure 1 shows values for perfectly smooth surfaces (i.e. mirror reflection), this behavior also strongly affects reflectance from rough

surfaces of the same materials.

### 3.2.2 Surface Scattering

The second important principle is the interaction with the wave nature of light. This is most obvious in diffraction gratings: features regularly spaced at intervals close to that of the light they reflect will actually diffract light in specific different directions. But random surfaces follow the same laws.

The simplest case is that of a perfectly smooth surface, which exhibits *ideal specular* or mirror-like reflection. Light reflected from such a surface retains its angular distribution, so such surfaces are used as mirrors. The only reason a “perfect” mirror is possible is the wave nature of light. If a surface has only roughness features significantly smaller than the wavelength, it appears smooth to those waves. This makes optical polishing possible: by grinding with successively finer grit, it is possible to reduce roughness to smaller than the wavelengths of interest. For visible light, roughness less than about  $0.02\mu\text{m}$  can be considered perfectly smooth. But for ultraviolet or X-rays, the same surface may be “rough”. Likewise, a surface that appears rough in the visible spectrum may be a smooth surface to infrared or microwave radiation.

Reflection from such a smooth surface was described by Fresnel in the 18th century. His equations predict that the reflectance of a smooth surface depends only on the incidence angle and the refractive index  $n$  of the material. The distinction between metals and dielectrics is maintained here in the value of  $n$ , which is a real number for dielectrics and a complex number for metals. Figure 1 shows the Fresnel reflectance as a function of angle for several typical metals and typical dielectrics. Some models ignore this angular variation of Fresnel reflectance, using a fixed value for all angles; we can anticipate that such models are better suited to modeling metals than dielectrics.

Surfaces with very small roughness are similar in behavior to perfectly smooth surfaces, but their specular reflectance is attenuated by a well-known relationship[Davies 1954]:

$$\rho \approx F e^{-\left(4\pi\frac{\sigma}{\lambda}\cos\theta_i\right)^2} \quad (1)$$

where  $\rho$  is the resulting specular reflectance,  $F$  is the Fresnel reflectance,  $\sigma$  is the RMS roughness height,  $\lambda$  is the wavelength of incident light, and  $\theta_i$  is the angle of incidence of that light. The fraction of light not

reflected into the mirror direction,  $F - \rho$ , is essentially scattered to the rest of the hemisphere above the surface. It is clear from Equation 1 that such slightly rough surfaces resemble perfectly-smooth surfaces in two cases: as  $\frac{\sigma}{\lambda}$  decreases, and as the angle of incidence approaches grazing at  $90^\circ$ . In either case, the term  $\frac{\sigma}{\lambda} \cos \theta_i$  approaches zero, feeding all energy into the ideal specular (mirror-like) reflection. The product  $\sigma \cos \theta_i$  is sometimes called the *apparent or effective roughness*, as sketched in Figure 2.

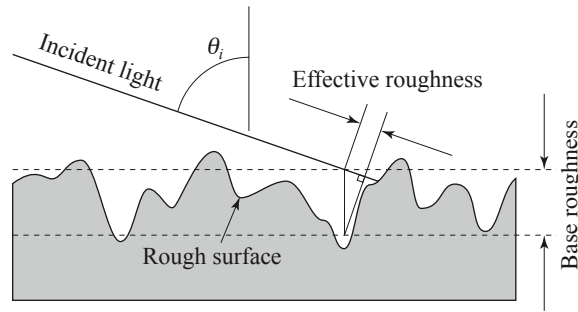


Figure 2: Effective roughness decreases according to  $\sigma \cos \theta_i$  as in Equation 1.

At the opposite extreme from smooth and slightly rough surfaces is the case where the roughness is much greater than the wavelength. Most reflectance models in computer graphics have been intended to operate in this regime, starting with Phong[1975] and including those of Ward[1992] and Cook and Torrance[1982]. For such surfaces, surface scattering takes the form of a smooth lobe at or near the specular direction; since  $\frac{\sigma}{\lambda}$  is large, specular (or mirror-like) reflection from the surface is neglected. Extremely rough surfaces such as sandpaper are not matched well by these rough-surface models, since they violate the assumptions of these models by having a large mean surface slope. Surfaces like unglazed ceramic and flat house paint show similar large-slope effects, and Oren and Nayar[1994] developed a model for these cases. This paper will not deal with large-slope surfaces.

A more complex case is that where the size of surface roughness approaches that of the wavelength, a case intermediate between the slightly rough and very rough extremes. The reflection behavior of such surfaces, surprisingly, is not a smooth transition of a rough-surface model to that of the smooth-surface model, but instead a superposition of the two separate cases. Such surfaces can only be handled by a full physical-optics model like that of He et al.[1991] or Stam[1999].

All rough surfaces, from slightly rough to very rough, actually behave as though their roughness varies

with the angles of illumination and reflection. When a surface is illuminated or viewed from extreme angles, the surface behaves as though it were smoother (see Figure 2). Further, if the roughness slopes are large enough, part of the roughness valleys can be occluded for both illumination and viewing, making the surface appear even smoother. Such behavior is visible in the real world. For example, rough pavement shows significant glare from headlights at night, since the incidence and viewing angles approach grazing. Rough paper, though normally highly diffuse, shows a sheen as viewing angles approach grazing. Because of this effect, certain surfaces can behave as either rough or smooth, depending on the angles of incidence and reflection. This effect is accounted for in the He-Torrance model, but is ignored in most other models.

### **3.2.3 Subsurface Scattering**

Even the best model of surface scattering is insufficient to reproduce the appearance of most surfaces, since much of the appearance (e.g. color) comes from scattering beneath the surface, within the body of the material. The only exceptions are metallic surfaces and black dielectrics. A metallic surface prevents subsurface scattering, since energy is absorbed within a fraction of one wavelength of the surface. A black dielectric also absorbs all energy that enters, but over a longer length scale. All other dielectric surfaces reflect significant energy via subsurface scattering.

Fortunately, two large classes of subsurface scattering can be modeled simply. Surfaces in the first class show diffuse subsurface scattering: the amount of subsurface scattering is practically independent of angle. Strictly speaking, the surface scattering will modify this pure behavior, as pointed out by Shirley et al.[1997], but often this can be neglected, as we will see in Section 4. The second class is metallic paints, which display a subsurface lobe much like that seen from rough surfaces. For such surfaces, we can press a rough-surface model into service.

## **4 Model Comparisons**

In this section we take several examples of surfaces that fit within our domain and fit four different models to reflectance measurements of each, applying the principles of Section 3 to explain the differences in performance.

Reflectance from a surface can be completely described by the BRDF, which is a 3D function for these surfaces, but we will examine the function only the plane of incidence, as this simplifies the process while still showing major differences between the models. The profile in the incidence plane defines the size, brightness, and position of the highlight from a small light source. The third dimension, the azimuth angle, determines the shape of the highlight, which is also important, but secondary.

We chose to plot data for three angles of incidence:  $10^\circ$ ,  $45^\circ$ , and  $75^\circ$ . This shows both the “typical” behavior at near-normal angles, the effects near grazing, and the transition between the two. Many evaluations of BRDF models and data omit angles near grazing, as both measurement and modeling become more difficult there, but this is the regime that shows the greatest differences between models.

The range of values of the BRDF is large, and a linear scale would completely obliterate the effects seen at low angles of incidence, so we have chosen to plot the data on a logarithmic scale. In addition, human perception of luminance is nonlinear, and the logarithmic scale follows Weber’s law [Wyszecki and Stiles 1982], a well-known approximation to this nonlinearity. This means that a given vertical distance on these graphs corresponds roughly to a similar perceptual difference.

We chose four models from the computer graphics literature for this comparison: the empirical models of Phong [1975] and Ward [1992], the physical model of He, Torrance, et al. and, as an example of the mathematical fitting approach, the representation of Lafortune et al. The measured BRDF comparison data were obtained with one calibrated gonioreflectometer, except for the surface of Section 4.4, which was measured by Marx and Vorberger [1990]. Renderings were generated by a Monte Carlo path tracer, including full global illumination for all transport paths. We present the five example surfaces in order of increasing complexity.

## **4.1 Rough Metal**

Our first sample is a rough aluminum surface, created by coating a sheet of anti-glare picture frame glass with pure aluminum; its visual appearance is typical for a rough metal surface, as shown in Figure 3. The measured BRDF data are shown in Figure 4; they show a directional diffuse lobe with a small ideal specular (mirror-like) component emerging at an incidence angle of  $\theta_i = 75^\circ$ . This ideal specular component corresponds approximately to the mirror reflection relation, Equation 1, but its magnitude is relatively

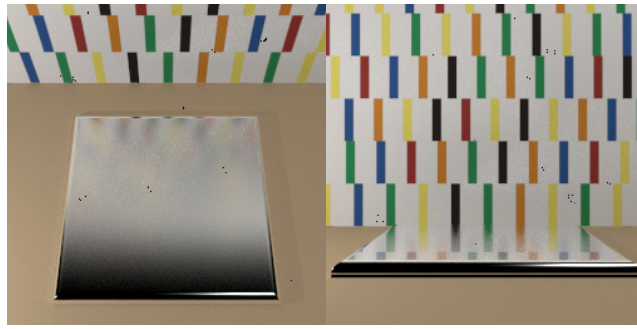


Figure 3: Renderings of rough aluminum surface at two viewing angles

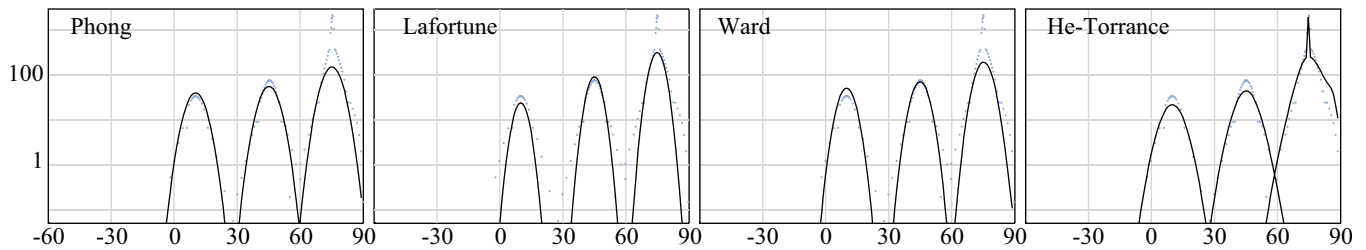


Figure 4: Fitting results for rough aluminum surface: BRDF vs. angle of reflection for three incidence angles,  $\lambda = 550nm$ .

small. Some mirror reflection is suggested in the right-hand rendering at the larger viewing angle in Figure 3. In Figure 4, three of the models seem to model only the narrower part of the directional diffuse lobe, while the He-Torrance model provides a better fit to the lobe and also predicts the emerging specular peak.

There is no striking difference in the performance of the four models for the directional diffuse lobes for this surface. The Phong model shows the least increase toward grazing incidence, but not much less than the other three models. It may be surprising to see any increase at all in the Phong model; the model was originally formulated in terms of radiance, but the BRDF is scaled by irradiance, which includes an extra term  $\cos \theta_i$ . Dividing by this term gives the increase shown in the directional diffuse lobe.

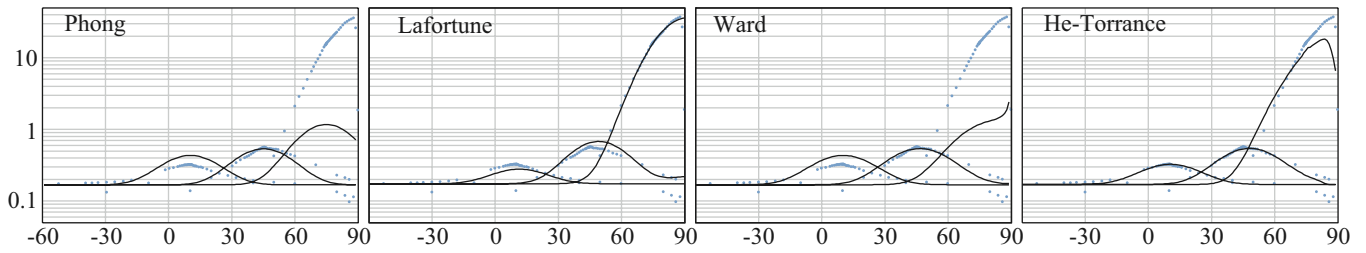


Figure 5: Fitting results for rough plastic surface: BRDF vs. angle of reflection for three incidence angles,  $\lambda = 550nm$ .

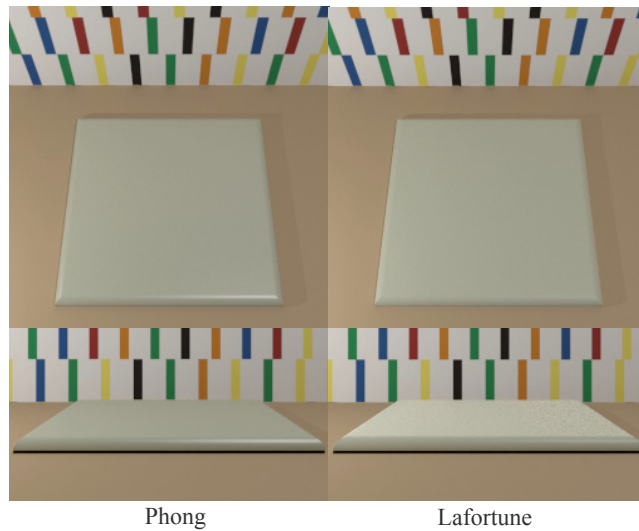


Figure 6: Comparison of rendered images of off-white rough plastic for two reflectance models.

## 4.2 Rough Plastic

We now move from a metallic surface to a dielectric: a section of an off-white computer case, which shows a finish with a slight sheen. An example rendering appears in Figure 6. The BRDF data are shown in Figure 5. Both this surface and the rough metal in Figure 4 show a directional diffuse lobe, but several differences are apparent. First, the minimum BRDF value in Figure 5 is much higher than in Figure 4; this is a constant Lambertian component due to subsurface scattering, and results in the off-white color of the surface. Second, the magnitude of the directional diffuse lobe varies much more with incidence angle for the dielectric surface, since it is a dielectric material and its Fresnel reflectance varies dramatically with angle, as shown in Figure 1. Third, the magnitude of the directional diffuse lobe is roughly a full order

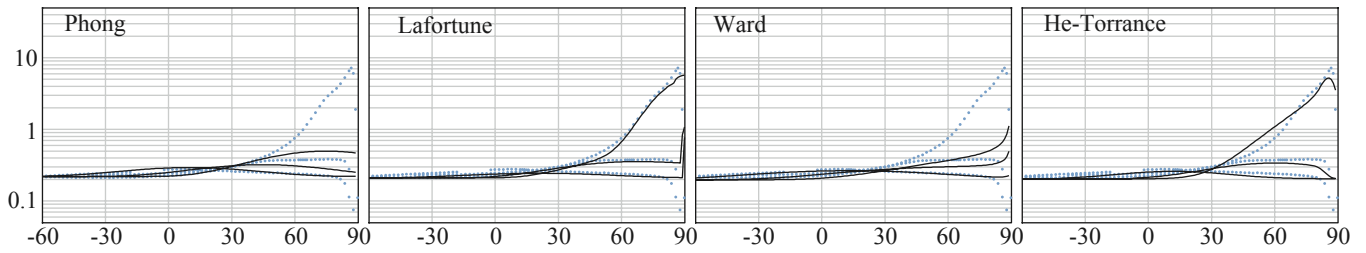


Figure 7: Fitting results for plain white paper: BRDF vs. angle of reflection for three incidence angles,  $\lambda = 550nm$ .

of magnitude less for the dielectric surface. The two surfaces show similar brightness, however, since the wider directional diffuse lobe and the constant Lambertian subsurface component of the plastic surface spread a similar amount of energy over a broader angular range. Finally, the wider directional diffuse lobe indicates a greater mean roughness slope on the plastic surface. This surface also shows no emergence of an ideal specular peak, indicating that the surface roughness  $\sigma$  is larger than that for the metal surface.

This material shows dramatic differences between the four models. The He-Torrance model fits well, but the Phong model cannot model the increase in the directional diffuse lobe. The Ward model also shows an inadequate increase toward grazing. The rate of increase toward grazing is fixed in the Ward model, whereas the He-Torrance model includes an explicit factor for the Fresnel reflectance and so models the increase. The Lafortune fitting model, as we might expect, has sufficient flexibility to reproduce the effect accurately. To see the visual effects of this difference, we have rendered a simple environment using two of the models and show the results in Figure 6. Notice how the Phong model is slightly brighter than the Lafortune model at viewing angles near normal, but much dimmer near grazing, where both the Fresnel reflectance and the reduced effective roughness increase the directional reflectance.

### 4.3 White Paper

This example is an ordinary sheet of office paper. It has a Lambertian subsurface scattering component, much like the rough plastic surface. The reflectance is shown in Figure 7. Unlike the plastic, there is no significant directional diffuse lobe at incidence angles near normal. Because of this, this surface might normally be modeled as purely Lambertian. However, its reflectance in Figure 7 varies dramatically

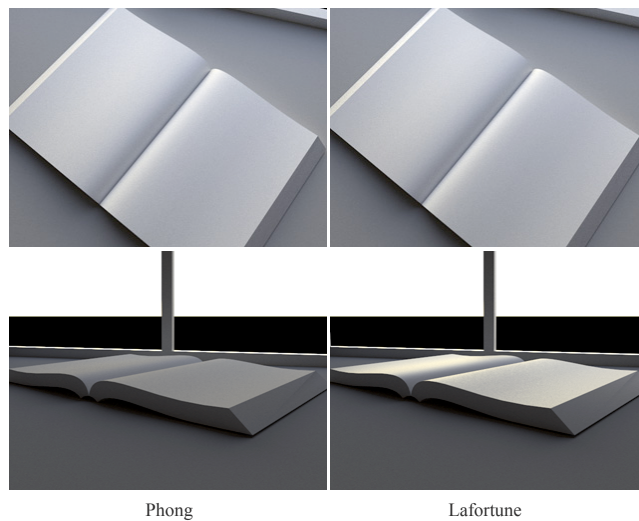


Figure 8: Comparison of rendered images of paper for two reflectance models

near grazing angles due partly to the decrease in effective roughness predicted by Equation 1. The He-Torrance model includes an effective roughness term, and models this increase well. The best fit, however, is offered by the Lafortune fitting model. The Phong and Ward models show dramatic departures from the true behavior. This is borne out in the renderings shown in Figure 8; near-normal viewing shows virtually no difference between the models, but viewing from near grazing shows a dramatic difference, with the Lafortune model looking much more natural. The golden color in the images is introduced by the illumination, which simulates a sunset sky.

#### 4.4 Smoother Metal

Our next example is a metal surface in the transition region between rough and smooth surface behavior. The surface, made of stainless steel and hand-lapped to near-mirror smoothness, was studied, and its reflectance measured, by Marx and Vorberger[1990]. We used the surface roughness statistics given in the paper: RMS roughness  $\sigma = 0.08\mu m$ , horizontal roughness  $\tau = 1.52\mu m$ . Since we were unable to obtain refractive index information for the stainless steel, we used the index for iron, the major component, but the behavior is relatively insensitive to this approximation. We have normalized both the measurement data from the paper and our BRDF results, as the data in the paper were not absolute; the result is shown in Figure 9. The specular peak is prominent even at the near-normal incidence angle of  $4^\circ$ , in contrast to

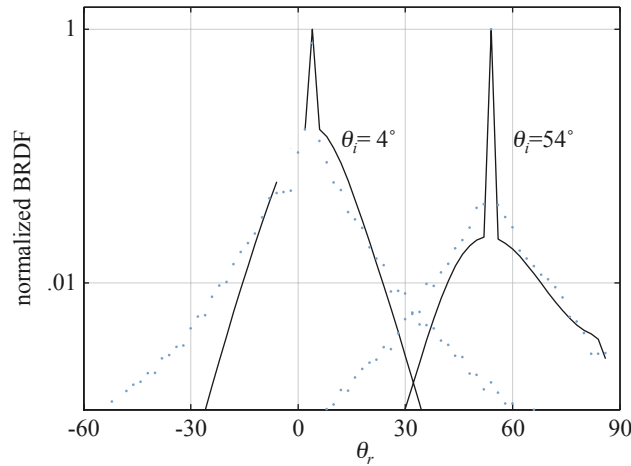


Figure 9: Fitting results for nearly-smooth metal surface: data from Marx et al., He-Torrance model,  $\lambda = 633nm$ .

the surface in Section 4.1, where it emerged only at large angles.  $\theta_i = 54^\circ$  is the largest incidence angle measured by Marx et al., but Equation 1 makes it clear that the specular component will grow still farther at greater incidence angles. We show only the results from the He-Torrance model, as none of the other models is capable of reproducing the ideal specular component. While the He-Torrance model does not exactly match the measurements, there is qualitative agreement, with the directional diffuse lobes similar in width and position over a range of two orders of magnitude.

Since the specular peak is so strong, it is tempting to model this material as a mirror, either by using the Fresnel reflectance or with a single reflectance value for all angles. This would, of course, save the computational complexity of the He-Torrance model. Figure 10 shows the result of this approach, compared to a rendering with the He-Torrance model. The most dramatic deficiency in the ideal mirror reflectance is the lack of the dramatic highlight from the sun, since its brightness is limited to a few pixels whose values are severely clipped. Traditionally this is handled by a non-physical model that provides a directional diffuse lobe such as Phong for light sources, as did Whitted[1980]. Unfortunately, there are subtler effects that would still be missing. Notice how the horizon is blurred on the front of the teapot in the right-hand image, but becomes perfectly distinct at the edge of the teapot, where angles approach grazing. Similarly, the reflection of the spout in the body of the teapot on the right is blurred in a way that is distinctive of slightly rough metal, such as the outside of an unpainted airliner.

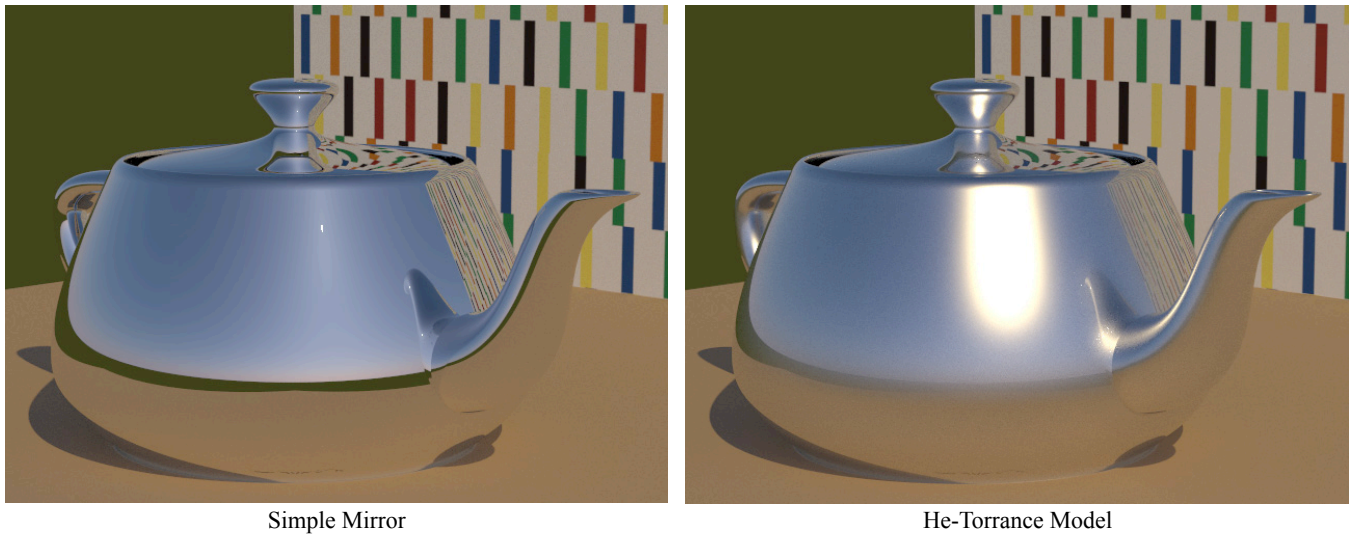


Figure 10: Renderings of nearly-smooth metal teapot

## 4.5 Metallic Paint

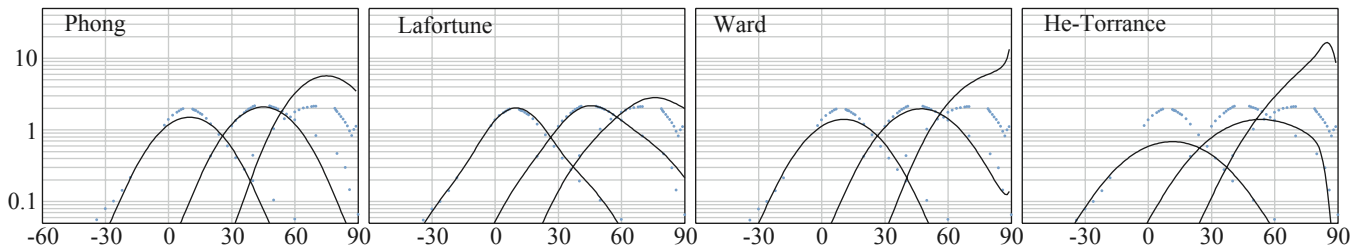


Figure 11: Fitting results for metallic paint with clearcoat: BRDF vs. angle of reflection for three incidence angles,  $\lambda = 550nm$ .

Our final example is an automotive metallic paint, showing how a more complex surface can be modeled with commonly-available models. In terms of the mechanisms of Section 3, this is most like the plastic surface of Section 4.2: it is a dielectric and shows important subsurface scattering. There are major differences, however. While the plastic surface is very rough, this paint has a very smooth, mirror-like surface. In addition, the subsurface scattering is very different from Lambertian. We show BRDF measurements of this paint in Figure 11. We have excluded the ideal specular reflection so as to observe the subsurface scattering; for rendering, the specular reflection can be modeled simply via the Fresnel equation.

The most interesting result is that the paint has a “metallic” visual appearance, but its reflectance is quite



Figure 12: Rendering using Lafortune model of metallic paint

different from that of a real metal. We see here a directional diffuse lobe that resembles the lobe from our rough aluminum sample, but shows very little variation with angle of incidence. This demonstrates a difficulty faced by the makers of the ill-fated Delorean automobile: it was impossible to paint the plastic body parts to match the stainless-steel body panels, since there is no paint that will match from all angles.

The Phong model reproduces this behavior well due its lack of variation with incidence angle. The Lafortune fitting model again shows the flexibility to match this performance, and the more sophisticated Ward and He-Torrance models are actually less accurate because this surface violates one of their assumptions. These models are intended to deal with a single material-air interface, not subsurface scattering modified by a mirror-like clear overcoat.

Figure 12 shows a car model rendered using the Lafortune model, with a Fresnel term added to describe the specular reflection from the clearcoat.

## **5 Application**

These results are interesting from an academic viewpoint, but they also can be applied in the real world when detailed measurements are not available. Since we have emphasized features that make a visible difference, we can make a reasonable choice of models for many surfaces based on direct visual observation of a surface. In many cases, this amounts to noting the amount of mirror reflection (if any) and the apparent surface finish, smooth or rough. Often the index of refraction  $n$  of the surface will be needed, and

in some cases, vertical and horizontal roughness lengths. To help achieve these objectives, the following guidelines are suggested.

The first guideline is simple:

*Use whatever data are available.*

If a diffuse reflectance measurement device is available, it can help to set diffuse parameters, especially the color effects, which vary with wavelength. If a photometer is available, it can be used to compare reflectance with a known reference. If a glossmeter is available, it can provide some directional information.

## 5.1 Estimating the Index of Refraction

When using a physically-based model such as Fresnel, He-Torrance or Cook-Torrance, it is necessary to choose a value for  $n$ , the index of refraction. If the composition of your surface is known, refractive index information may be available (e.g. Table 1); Palik's compilations[1985; 1998] are particularly useful.

The variation of the index of refraction across the visible spectrum is small for the metals in Table 1, and even smaller for the dielectrics. This means that we can start by setting a constant index  $n$ , and that the mirror reflection and any directional diffuse lobe from surface scattering will retain the color of the light source. The value of  $n$  can often be estimated from a single measurement, suggesting our next guideline:

*Some simple measurements may help.*

If a smooth sample of the material is available (e.g. a sheet of glass), a simple measurement of specular reflectance near normal incidence allows us to estimate  $n$ , as in Cook et al.[1982]:

$$n = \frac{1 + \sqrt{F_0}}{1 - \sqrt{F_0}} \quad (2)$$

where  $F_0$  is the Fresnel (ideal specular) reflectance at or near normal incidence. While this is only exact for dielectrics, we can, as did Cook, use this equation to estimate an equivalent real-valued  $n$  for metals by using the measured normal reflectance of the metals. The estimated Fresnel reflectance curve for the metals is then similar in shape to that of the dielectrics shown in Figure 1, but it is shifted to higher reflectance values at all angles of incidence.

If there are no reflectance data or physical parameters available for the surface being modeled, some rough estimates may suffice for both dielectrics and metals. We need not try all possible values since the index  $n$  is not totally arbitrary. This leads to our next guideline:

*Make intelligent guesses*

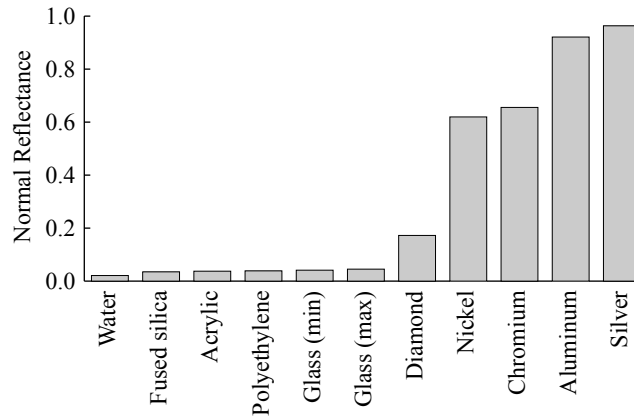


Figure 13: Specular reflectance at normal incidence for various materials

To help the reader estimate  $n$  for a dielectric surface, we have listed several common materials in the first section of Table 1. Most common dielectrics cluster around the value  $n \approx 1.5$ , leading to a normal reflectance of around 0.04. Diamond is included as a practical boundary for dielectrics. Its high index of refraction results in the bright glitter that makes it a valuable gemstone, but even this outlying case shows a normal reflectance in Figure 13 that is far below that of metals. This leads us to suggest:

*For most dielectrics, 1.5 is an adequate approximation to  $n$ .*

For water and ice, and many liquids,  $n$  will be less, reducing the normal reflectance; for gemstones or high-quality crystal, it will be higher, increasing reflectance at most angles.

For metals, the estimate of  $n$  is harder; a single reflectance measurement is inadequate for obtaining both components of the complex index. Fortunately, the Fresnel reflectance function is simpler in shape for metals, as seen in Figure 1: the reflectance remains within a small range over most of the angular domain. This leads us to suggest:

*For most metals, it is permissible to ignore the angular variation in Fresnel reflectance.*

This often allows the use of simpler models, e.g. a constant reflectance for a metal mirror or the Ward model for rough metal surfaces. It will still be necessary to estimate the magnitude of the constant reflectance used, and that might be based on a measured normal reflectance.

## **5.2 Directional Scattering**

Visual input to the modeling process helps in choosing a model. If the surface has a mirror-like finish, we can use the Fresnel equations or perhaps a constant value of the specular reflectance to model the reflection behavior. For surfaces of low gloss, the Ward model can be used for metals and the He-Torrance model is suitable for metals or dielectric materials. For high-gloss surfaces, the He-Torrance model is needed to capture the wave-optics effects correctly. Stam's method can also capture these effects, but assumes the Fresnel reflectance constant with angle, so it is best suited for metal surfaces.

In our comparisons in Section 4, and ignoring the wave-optics mirror reflection behavior, the major difference between the models is the rate of increase in the directional diffuse lobe with increasing angle of incidence. Thus we may draw our first guideline in choosing a reflectance model:

*The principal difference between models for rough-surface reflection is their rate of increase toward grazing.*

This means, surprisingly, that the most sophisticated or complex model may *not* be the best to use in a particular case, as with the metallic paint in Section 4.5, where the Phong model actually outperformed the Ward and He-Torrance models. In other cases, a comparison of the surface to be modeled against the five surfaces described in Section 4 will be helpful in choosing a model.

We must also decide how to model subsurface reflection. In this paper we have used three alternatives:

- Model the subsurface scattering as Lambertian
- Model the subsurface scattering with a general lobe (Phong)
- Omit subsurface scattering completely

The first option is valid for many paints and plastics: all those that show a solid color. The second option is valid for paints and plastics with a “metallic” look, as with many automotive finishes. The last option is valid both for metals and for surfaces whose base color is black.

When modeling Lambertian subsurface scattering, we need to estimate its magnitude. Perceived brightness is deceptive, as it is nonlinear with reflectance. The photographic standard for medium gray, for example, is 18%. A reflectance of 30% is actually a medium or light gray. Our white paper sample has a measured total reflectance of only about 75%. While accurate estimates of absolute magnitude are difficult, we can

*Estimate any Lambertian scattering by comparison with a scale of known diffuse reflectances.*

We have used the neutral patches of the Macbeth ColorChecker™ test chart, giving 5 patches with reflectance ranging from about 3.2% to about 89%. This allows us to estimate the diffuse reflectance of many surfaces by visual comparison. Of course, if a diffuse reflectometer is available, the reflectance can be measured almost directly.

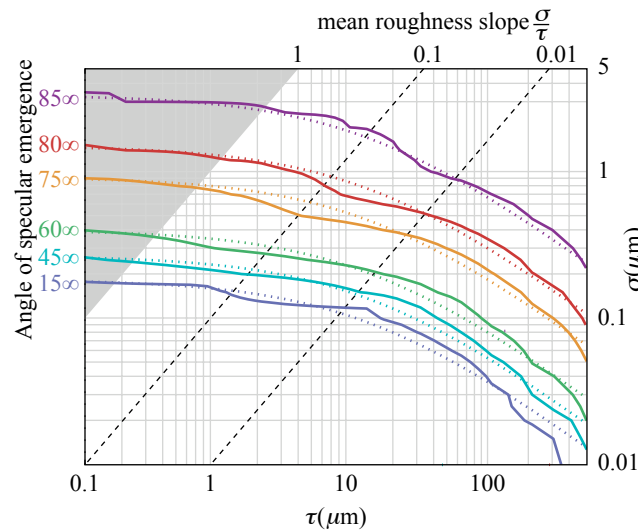


Figure 14: Specular transition vs. model parameters

We also need to adjust model parameters for surface roughness. Fortunately,

*Surface roughness parameters can often be estimated visually.*

Simpler models, such as the Ward, Phong, and Cook-Torrance models, require only a single parameter to control the directional-diffuse lobe width; this can be set visually with trial-and-error renderings. Wave-optics models, however, require some knowledge of the physical scale of surface roughness to control the emergence of mirror-like ideal specular behavior, but the model itself can help us turn visual observations into estimated parameters.

The surface roughness is usually described by the RMS vertical roughness  $\sigma$  and a horizontal roughness scale  $\tau$ . A simple measurement may be feasible; compact instruments are available that measure surface roughness using a mechanical stylus.

When no direct measurement of roughness is available, we can use a wave-optics model directly to estimate the roughness parameters. This requires that the specular emergence be visible. Figure 14 gives some guidance on how to set the parameters. The ordinate is the surface RMS roughness  $\sigma$  and the abscissa is the horizontal roughness  $\tau$ . Each colored curve shows the surface parameters at emergence of the specular component for a particular angle of emergence, as labeled along the left. Our criterion for this emergence was the point at which specular reflectance equals the directional diffuse reflectance in the specular direction, at a wavelength of 550nm, and with a viewing solid angle corresponding to the human eye at an arm's length distance from the surface to be modeled.

To use this diagram, we first observe the surface and measure the reflection angle at which the ideal specular component becomes visible to the eye. For example, suppose this angle is about  $80^\circ$ . We look along the left side of Figure 14 and find the red contour line corresponding to this angle. If we start by assuming a mean slope of 0.1, we follow this red contour to the point where it crosses the dashed line for  $\frac{\sigma}{\tau} = 0.1$ , which is at  $\sigma = 0.5\mu m, \tau = 5\mu m$ . This will serve as a starting point for visual experimentation, varying  $\sigma$  and  $\tau$  while remaining on the red contour. We have shaded the area where  $\frac{\sigma}{\tau} > 1.0$ , since this is beyond the regime where the He-Torrance model's assumptions hold. Most surfaces for which this model is applicable lie in the regime  $0.01 \leq \frac{\sigma}{\tau} \leq 1$ . For convenience, the relationship between  $\sigma$  and  $\tau$  in Figure 14 can be estimated by the empirical formula

$$\sigma = \frac{C}{\tau^{0.7} + 6}, \quad (3)$$

where  $C$  depends on the angle of observed specular emergence and  $\sigma$  and  $\tau$  are in micrometers. Values of

$C$  are tabulated in Table 2. The dotted lines in Figure 14 show the results of this estimate for each of the specular-emergence angles.

## 6 Conclusion

We have outlined a principled, yet practical, approach to visual modeling for many surfaces. Though based on physical measurements, the approach can be used even when no such measurements are available. We have demonstrated several principles that are vital to modeling the reflectance of a surface well, including:

- There are visible differences between various reflectance models
- No one model performs well on every surface
- Sometimes the most sophisticated model is not the best choice
- We can use guiding principles and rules of thumb to model surfaces better, even when specialized instrumentation is unavailable.

We have presented some guidelines to aid the practitioner in selecting a reflectance model for certain types of surfaces. Since these guidelines are based on physical measurements, they are more reliable than intuition based on individual renderings.

### 6.1 Further Work

The work should be continued in two ways: rigor and generality.

We have judged different models by visually comparing graphs with measured data and drawing gross distinctions that we feel are valid. We have not yet addressed the question of measurable perceptual differences in renderings: some of the differences seen in the graphs may not be detectable in a rendered image, or some of the the residual differences between the “good” models, or between them and the true data, may be perceptible.

We have also chosen to deal with only one class of surfaces: those that exhibit a smooth directional-diffuse reflectance lobe at or near the specular direction, giving the classic computer graphics highlight,

with possibly an additional mirror-like component. It will be a worthwhile challenge to apply a similar approach to surfaces that display retroreflection, anisotropy, and other phenomena.

This paper is intended only as a next step; much remains to be done, including:

- Evaluating the performance of these models out of the plane of incidence
- Extending the classes of surfaces studied: e.g. retroreflective paints, rough ceramics, velvet
- Evaluating more models, e.g. Oren-Nayar
- Using the insights to design new models that combine the intuitive interaction of Phong with better reproduction of visual effects

## References

- BLINN, J. F. 1977. Models of light reflection for computer synthesized pictures. vol. 11, 192–198.
- BORSHUKOV, G. 2003. Measured BRDF in film production: Realistic cloth appearance for "the matrix reloaded". In *SIGGRAPH 2003 Sketches and Applications*.
- BROWN, G. A. 1985. Factors affecting the refractive index distribution of window glass. *Journal of Forensic Sciences* 30, 3 (July), 806–813.
- COOK, R. L., AND TORRANCE, K. E. 1982. A reflectance model for computer graphics. *ACM Transactions on Graphics* 1, 1 (Jan.), 7–24.
- CORNELL UNIVERSITY PROGRAM OF COMPUTER GRAPHICS, 1999. Measurement data. <http://www.graphics.cornell.edu/online/measurements/>.
- DANA, K. J., GINNEKEN, B. V., NAYAR, S. K., AND KOENDERINK, J. J., 1997. Columbia-utrecht reflectance and texture database. <http://www1.cs.columbia.edu/CAVE/curet/>.
- DAVIES, H. 1954. The reflection of electromagnetic waves from a rough surface. *Proc. IEE* 101, 209–214.
- HE, X. D., TORRANCE, K. E., SILLION, F. X., AND GREENBERG, D. P. 1991. A comprehensive physical model for light reflection. In *Computer Graphics (Proceedings of SIGGRAPH 91)*, vol. 25, 175–186.
- KAJIYA, J. T. 1985. Anisotropic reflection models. In *Computer Graphics (Proceedings of SIGGRAPH 85)*, vol. 19, 15–21.
- KAUTZ, J., AND MCCOOL, M. D. 1999. Interactive rendering with arbitrary BRDFs using separable approximations. In *Eurographics Rendering Workshop 1999*.

## Online Submission ID:

- KOENDERINK, J., AND VAN DOORN, A. 1998. Phenomenological description of bidirectional surface reflection. *J. Opt. Soc. Am. A* 15, 11 (Nov.), 2903–2912.
- LAFORTUNE, E. P. F., FOO, S.-C., TORRANCE, K. E., AND GREENBERG, D. P. 1997. Non-linear approximation of reflectance functions. In *Proceedings of SIGGRAPH 97*, Computer Graphics Proceedings, Annual Conference Series, 117–126.
- LALONDE, P., AND FOURNIER, A. 1997. A wavelet representation of reflectance functions. *IEEE Transactions on Visualization and Computer Graphics* 3, 4 (October–December), 329–336.
- LEWIS, R. 1993. Making shaders more physically plausible. In *Fourth Eurographics Workshop on Rendering*, 47–62.
- MARX, E., AND VORBERGER, T. V. 1990. Direct and inverse problems for light scattered by rough surfaces. *Applied Optics* 29, 25 (Sept.), 3613–3626.
- MATUSIK, W., PFISTER, H., BRAND, M., AND MCMILLAN, L. 2003. A data-driven reflectance model. *ACM Transactions on Graphics* 22, 3 (July), 759–769.
- OREN, M., AND NAYAR, S. K. 1994. Generalization of lambert’s reflectance model. In *Proceedings of SIGGRAPH 94*, Computer Graphics Proceedings, Annual Conference Series, 239–246.
- PALIK, E. D., Ed. 1985. *Handbook of Physical Constants of Solids*. Academic Press.
- PALIK, E. D., Ed. 1998. *Handbook of Physical Constants of Solids*. Academic Press.
- PHONG, B.-T. 1975. Illumination for computer generated pictures. *Communications of the ACM* 18, 6 (June), 311–317.
- POULIN, P., AND FOURNIER, A. 1990. A model for anisotropic reflection. In *Computer Graphics (Proceedings of SIGGRAPH 90)*, vol. 24, 273–282.
- SCHRÖDER, P., AND SWELDENS, W. 1995. Spherical wavelets: Efficiently representing functions on the sphere. In *Proceedings of SIGGRAPH 95*, Computer Graphics Proceedings, Annual Conference Series, 161–172.
- SEGELSTEIN, D. J. 1981. *The complex refractive index of water*. Master’s thesis, University of Missouri-Kansas City.
- SHIRLEY, P., HU, H., SMITS, B., AND LAFORTUNE, E. P. 1997. A practitioners’ assessment of light reflection models. In *Pacific Graphics ’97*.
- SILLION, F. X., ARVO, J. R., WESTIN, S. H., AND GREENBERG, D. P. 1991. A global illumination solution for general reflectance distributions. In *Computer Graphics (Proceedings of SIGGRAPH 91)*, vol. 25, 187–196.
- STAM, J. 1999. Diffraction shaders. In *Proceedings of SIGGRAPH 99*, Computer Graphics Proceedings, Annual Conference Series, 101–110.

## *Online Submission ID:*

- WARD, G. J. 1992. Measuring and modeling anisotropic reflection. *Computer Graphics* 26, 2 (July), 265–272. Proceedings of SIGGRAPH '92.
- WESTIN, S. H., ARVO, J. R., AND TORRANCE, K. E. 1992. Predicting reflectance functions from complex surfaces. In *Computer Graphics (Proceedings of SIGGRAPH 92)*, vol. 26, 255–264.
- WESTLUND, H. B., AND MEYER, G. W. 2001. Applying appearance standards to light reflection models. In *Proceedings of ACM SIGGRAPH 2001*, Computer Graphics Proceedings, Annual Conference Series, 501–510.
- WHITTED, T. 1980. An improved illumination model for shaded display. *Communications of the ACM* 23, 6 (June), 343–349.
- WYSZECKI, G., AND STILES, W. S. 1982. *Color Science: Concepts and Methods, Quantitative Data and Formulae*, second edition ed. John Wiley and Sons, ch. 6, 490.

Material	$n$	Normal Re- flectance	Source
Water	$\approx 1.34$	0.0211	[Segelstein 1981]
Fused silica (pure glass)	1.460 (at 546.074nm)	0.0350	[Palik 1985]
Lucite® acrylic	$\approx 1.48$	0.0375	Our measurement
Polyethylene	1.490 (at 551.1nm)	0.0387	[Palik 1985]
Window glass	1.51-1.54	0.0413- 0.0452	[Brown 1985]
Diamond	2.4203	0.1724	[Palik 1985]
Nickel	1.80 + 3.33 <i>i</i> (at 563.6nm)	0.6196	[Palik 1985]
Chromium	3.18 + 4.41 <i>i</i> (at 558.5nm)	0.6555	[Palik 1998]
Aluminum	0.958 + 6.69 <i>i</i>	0.9211	[Palik 1985]
Silver	0.120 + 3.45 <i>i</i>	0.9635	[Palik 1985]

Table 1: Refractive indices of a few common materials,  $\lambda = 550nm$

Angle	15°	45°	60°	75°	80°	85°
$C$	1.1	1.6	2.4	5.5	9	20

Table 2: Values of Empirical Constant  $C$